Available online at www.sciencedirect.com
ScienceDirect
Trans. Nonferrous Met. Soc. China 33(2023) 2340−2350
Transactions of Nonferrous Metals Society of China
www.tnmsc.cn

Effects of heat treatment on microstructure and tensile mechanical properties of isothermal die forged AZ80−Ag casing with large size

Fei-teng CHEN[1], Shu-nong JIANG[1], Zhi-yong CHEN[1], Chu-ming LIU[1,2]

1. School of Materials Science and Engineering, Central South University, Changsha 410083, China;
2. School of Materials Science and Engineering, Hunan University of Science and Technology, Xiangtan 411201, China

Received 13 March 2022; accepted 27 May 2022

Abstract: The microstructure evolution and tensile mechanical properties of the isothermal die forged AZ80−Ag casing with large size under different heat treatment conditions were investigated. The microstructure was characterized by scanning electron microscope and electron backscatter diffraction techniques, and the tensile mechanical properties were tested at room temperature, 120 and 150 °C, respectively. The results show that the area fraction of discontinuous precipitates with stronger strengthening effect is higher in T5 sample than that in T6 sample, therefore T5 sample exhibits a more pronounced precipitation hardening and the highest tensile strength at room temperature. However, as the temperature increases, the tensile strength of T5 sample decreases rapidly and is lower than that of T6 sample or even the as-forged samples at 150 °C. The reason is that discontinuous precipitates are less resistant to high temperature softening than continuous precipitates.

Key words: AZ80−Ag alloy; heat treatment; elevated temperature tensile properties; discontinuous precipitates; precipitation hardening

1 Introduction

As the lightest metal structure material, magnesium alloys have attracted more and more attention in automotive and aerospace areas due to the demand of weight reduction [1]. Among various magnesium alloy systems, AZ80 is a widely used medium-strength magnesium alloy with excellent comprehensive mechanical properties and low cost [2]. However, as a precipitation-hardened alloy, AZ80 exhibits a weak aging hardening response [3]. Moreover, the application of AZ80 in elevated temperature service conditions is limited due to its poor heat resistance [4]. In recent years, AZ80−Ag, a new magnesium alloy developed by the author's team by adding trace Ag into AZ80, exhibits enhanced age-hardening response and improved heat resistance [5,6]. Therefore, AZ80−Ag is an ideal material for magnesium alloy components with low cost and high performance, and has a wide application prospect.

In addition, the practical application of magnesium alloys is also limited by their poor formability and strong mechanical anisotropy at room temperature because of the hexagonal close-packed crystal structure [7]. As a result, the current industrial production of magnesium alloy components is limited to conventional extrusion, rolling and forging processes, which is difficult to meet the actual demand for complex-shaped components. Isothermal die forging is characterized by heating the dies and keeping the same temperature as the billet during the forging process, which can significantly improve the workability and flowability of metals, thus obtaining forgings with complex shapes, fine-grained microstructure and excellent mechanical properties [8]. It has also

Corresponding author: Shu-nong JIANG, Tel: +86-13687372564, E-mail: shnjiang@csu.edu.cn
DOI: 10.1016/S1003-6326(23)66263-6

been successfully applied to manufacturing high-performance magnesium alloys with large size and complex shape [9−13]. However, the current research has mainly focused on the finite element simulation of isothermal die forging, but little has studied subsequent heat treatment, which is regarded as a crucial process to further improve mechanical properties of magnesium alloys. ZHAO et al [2] studied the microstructure evolution and tensile properties of extruded AZ80 under different heat treatment conditions. The results showed that T5 treatment achieved the highest strength, but the elongation significantly decreased, and appropriate T6 treatment could obtain an improved combination of strength and elongation. UEMATSU et al [14] reported that T5 treatment improved the tensile strength and high-cycle fatigue strength of extruded AZ80. ZHAO et al [15] examined the low-cycle fatigue of extruded AZ80 and observed the improved fatigue life of T5 peak-aged sample at medium strain amplitudes (0.3%−0.8%). However, only a few studies focused on the effect of heat treatment on elevated temperature mechanical properties.

The isothermal die forged AZ80−Ag disk for areoengine casing studied in this work has a large size and complex shape, which has never been done before. In order to promote its application in aerospace field, an understanding of the microstructure and tensile properties at room and elevated temperatures, and their response to heat treatment for the forged AZ80−Ag are required.

2 Experimental

The object investigated in this work was an AZ80−Ag (Mg−8Al−0.4Zn−0.2Mn−0.2Ag in wt.%) magnesium alloy disk with a diameter more than 560 mm prepared by isothermal die forging at 370 °C. The disk was then cut into four parts, three of which were subjected to different heat treatments (details are summarized in Table 1). Considering the practical application, the web of disk was specifically studied. The schematic of sampling locations and orientations of tensile specimens in the disk is shown in Fig. 1, where RD, TD and ND represent radial direction, tangential direction and normal direction, respectively. For convenience, samples from the as-received part were defined as as-forged, and samples from the heat-treated parts were labeled as T4, T5 and T6.

Table 1 Heat treatment schedule for disk

Designation	Heat treatment schedule
Solution treatment (T4)	Solution at 410 °C for 3.5 h followed by water quenching
Direct-aging treatment (T5)	Aging at 175 °C for 36 h followed by air-cooling
Solution + aging treatment (T6)	(Solution at 410 °C for 3.5 h, water quenching) + (aging at 175 °C for 36 h, air-cooling)

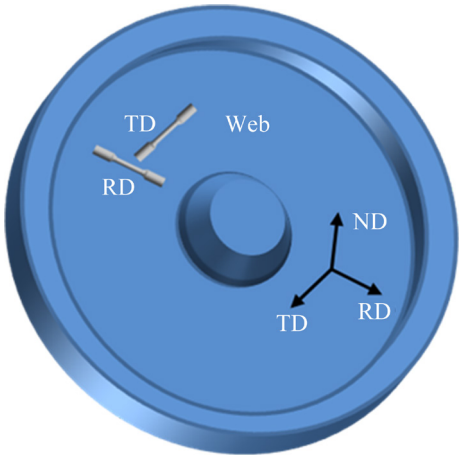

Fig. 1 Schematic of sampling locations and orientations of tensile specimens in web of disk

EBSD measurements were carried out to identify the grain orientation and texture features in an FEI Helios Nanolab 600i dual beam electron microscope equipped with HKL Channel 5.0 software. The EBSD samples were firstly mechanically polished, followed by electro-polishing in a solution of 4 vol.% perchloric acid, 1 vol.% nitric acid and 95 vol.% ethanol at 25 V and −40 °C for 90 s. The microstructure was characterized using a Tescan Mira SEM. The SEM samples were prepared by mechanically polishing, etching with a solution of oxalic acid (1 g), nitric acid (1 mL), acetic acid (1 mL) and distilled water (100 mL) for 10 s, and subsequent ultrasonic bath cleaning with ethanol. The area fractions of discontinuous precipitates (DPs) and continuous precipitates (CPs) regions were calculated with the Image-Pro Plus software from at least 5 SEM pictures at 500 times magnification. Tensile tests were performed at room temperature, 120 and 150 °C using an Instron 3369 universal testing machine with a strain rate of $1.5\times10^{-3}\ s^{-1}$. The tensile specimens, with the gauge dimensions of *d*5 mm × 25 mm, were electro- discharge machined from the web of the disk along the TD and RD.

3 Results and discussion

3.1 Microstructure and precipitation behaviors of as-forged and T4 samples

Figure 2 shows the inverse pole and pole figures of the as-forged and T4 samples. The temperature of aging treatment is relatively low, which has almost no effect on the grain size and texture, so T5 and T6 samples are not shown. In the as-forged sample, the microstructure consists of alternating fine-grained and coarse-grained region parallel to the RD with a wide grain size distribution and an average size of 19.3 μm (Fig. 2(a)). A large number of low-angle grain boundaries (2°−15°, white lines) and color gradient within the grains can also be observed in Fig. 2(a), reflecting the misorientation caused by dislocation accumulation, which are typical microstructure characteristics of the continuous dynamic recrystallization (CDRX) [16,17]. Also, the sample shows a bimodal texture with a high I_{max} (maximum intensity) of 19.2 MRD (multiples of a random density), as shown in Fig. 2(b). In addition to a strong texture component with *c*-axis approximately parallel to the ND, a sub-strong basal texture component is also observed. In the case of T4 sample, the average grain size reaches 60.8 μm (about 3 times that of the as-forged sample) after static recrystallization and grain growth, but the microstructure still remains heterogeneous (Fig. 2(c)). Similarly, Fig. 2(d) shows that the texture maintains the same bimodal feature, only with a slightly lower I_{max} of 16.8 MRD, suggesting that T4 treatment has a negligible effect on the texture.

Figure 3 presents the SEM images of the as-forged and heat-treated samples. In the as-forged sample, two groups of precipitates are observed: (1) the dominant group is the fine *β*-phase particles that form precipitate bands parallel to the RD; (2) the minor group is relatively coarse and sporadically distributed Al−Mn phases (Fig. 3(a)). The formation of precipitate bands can be attributed to the inhomogeneous distribution of Al atoms dissolved in the matrix, which leads to the dynamic precipitation of *β*-phase particles in the region with high Al content during isothermal die forging [2]. Furthermore, metal flow in the web is along the RD, so the precipitate bands are also formed parallel to the RD [11,18]. A high-magnification SEM image of the precipitate bands is shown in Fig. 3(b). It can be seen that precipitate bands coincide with the fine-grained region and fine *β*-phase particles are mostly distributed along grain boundaries, which indicates that fine grains origin from dynamic recrystallization (DRX) and the *β*-phase particles play an important role in restricting

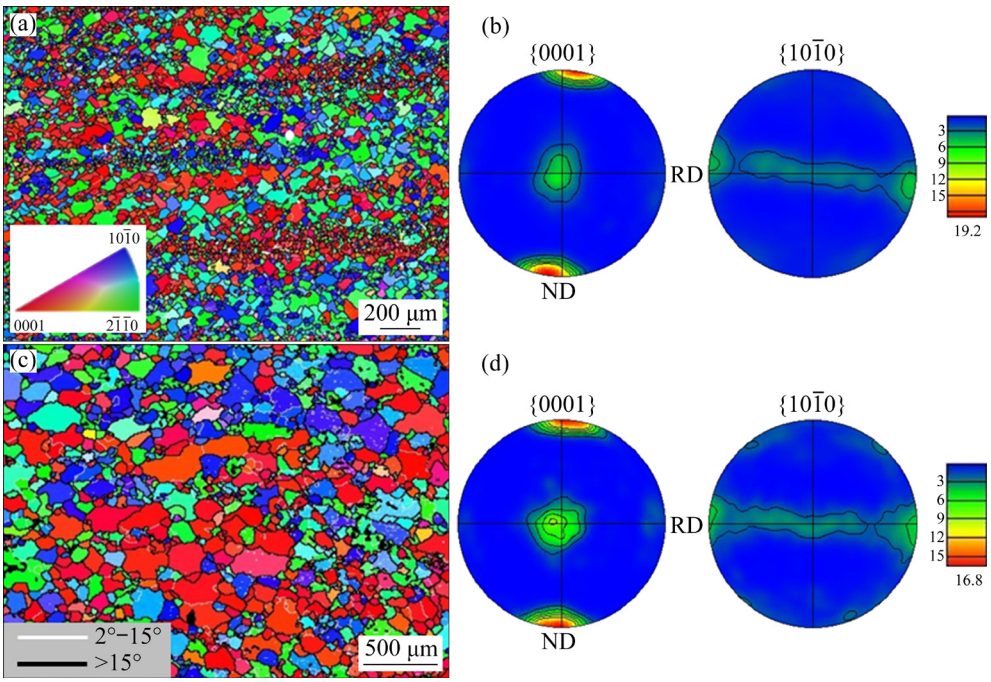

Fig. 2 Inverse pole (a, c) and pole (b, d) figures of as-forged (a, b) and T4 (c, d) samples

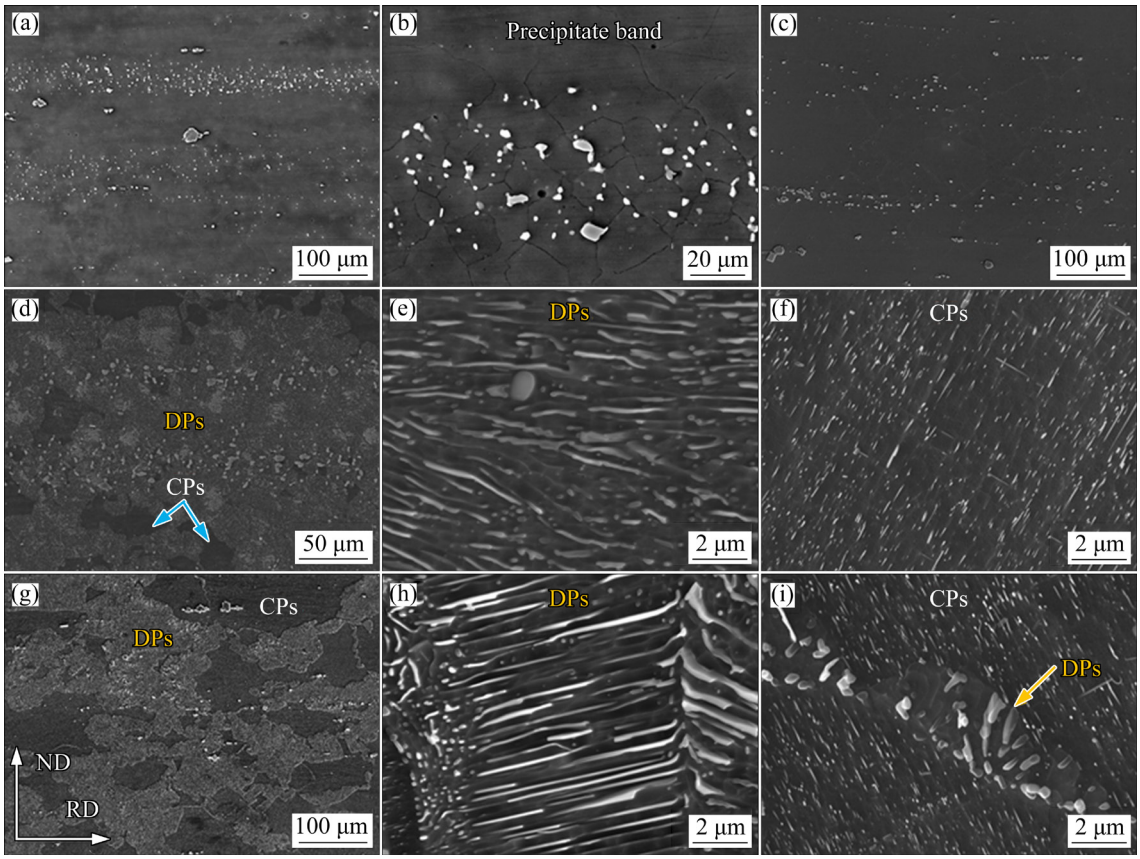

Fig. 3 SEM micrographs of as-forged (a, b), T4 (c), T5 (d−f) and T6 (g−i) samples

grain growth by the pinning effect [7,19]. After T4 heat treatment (as shown in Fig. 3(c)), β-phase particles almost completely dissolve into the matrix and precipitate bands disappear, while Al−Mn phases are still observed for their high thermal stability. Considering the fact that the area fraction of Al−Mn phases is negligible, they can hardly affect the precipitation behavior and mechanical properties of aged samples.

In Mg−Al alloys, the main precipitates, β-$Mg_{17}Al_{12}$, can be distinguished into two categories according to modes they are formed: DPs and CPs [20,21]. DPs nucleate mainly at the grain boundaries and grow perpendicularly into the grains, while CPs form later within grains. In the SEM image of the T5 sample (Fig. 3(d)), the precipitate bands still remain, while most of the area is occupied by DPs (bright contrast) and a small amount of CPs (dark contrast) are detected in DPs-free area. SEM micrographs taken in the DPs and CPs regions of the T5 sample are shown in Figs. 3(e) and (f), respectively. It can be seen that precipitates exhibit the typical morphological features of DPs and CPs in Mg−Al alloys, i.e. lamellar and elliptical DPs, and lath-shaped CPs. Similarly, the microstructure of the T6 sample is also mainly composed of DPs and CPs, between which DPs are dominant in the area fraction (Fig. 3(g)). In addition, the typical precipitation morphologies of DPs and CPs are also identified in the T6 sample (Figs. 3(h) and (i), respectively). The difference is that the area fraction of DPs in the T5 sample (84%) is higher than that in the T6 sample (61%), which is related to the microstructure of pre-aged samples and the characteristics of discontinuous precipitation and continuous precipitation.

On the one hand, the nucleation of DPs occurs at grain boundaries, so the as-forged sample with smaller average grain size has higher area fraction of grain boundaries that act as nucleation sites [22]. Moreover, the second phases in the as-forged sample lead to the segregation of Al atoms and constituent fluctuation, which is conducive to the formation of DPs during subsequent aging process (obtaining T5 sample). When the area fraction of DPs is sufficient, the formation of CPs will be effectively inhibited [23]. Therefore, CPs can

hardly be seen in the precipitate band region (Fig. 3(d)), which is similar to the phenomenon observed in previous studies [2]. On the other hand, the nucleation of CPs occurs inside grains and is sensitive to the supersaturation degree of Al atoms in the matrix [2,24]. Most of the second phases are dissolved in the matrix and supersaturated solid solution is obtained after T4 treatment, which promotes the formation of CPs during subsequent aging process (obtaining T6 sample). Furthermore, CPs can inhibit the growth of DPs by reducing supersaturation [23], such as the DPs that terminate growth prematurely in Fig. 3(i).

3.2 Tensile mechanical properties of as-forged and heat-treated samples at room temperature

The tensile engineering stress−strain curves of the as-forged and heat-treated samples at room temperature with loading direction parallel to the TD and RD are shown in Figs. 4(a) and (b), respectively. Simultaneously, the yield strength (YS), ultimate tensile strength (UTS), elongation (EL) and the difference of YS along the RD and TD

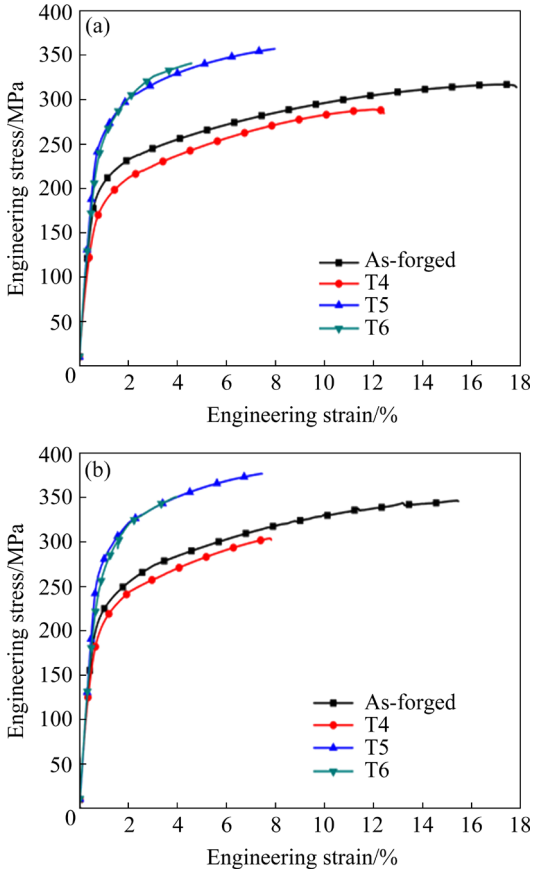

Fig. 4 Typical tensile engineering stress−strain curves of as-forged and heat-treated samples at room temperature with loading direction parallel to TD (a) and RD (b)

(ΔYS) measured from the tensile curves are presented in Table 2. It is obvious that mechanical anisotropy exists in the as-forged tensile specimens, in which the ΔYS reaches 35 MPa. In general, mechanical anisotropy is closely related to the activation of different deformation mechanisms during tension, which can be estimated by the Schmid factor associated with texture feature. Basal slip is usually the dominant deformation mechanism in magnesium alloys at room temperature due to its lowest critical resolved shear stress (CRSS) [25]. However, it has been widely reported that tensile twinning and prismatic slip with higher CRSS may also be activated when favorable texture is present [7,26−28]. In this work, the main texture component of the as-forged sample is unfavorable for tensile twinning, but is in favor of prismatic slip, whether stretching along the TD or RD (Fig. 2). Hence, only basal slip and prismatic slip are considered as the potential dominant deformation modes, and their Schmid factor distribution maps for the as-forged sample along the TD and RD are plotted in Figs. 5(a) and (b), respectively. The corresponding average Schmid factors are also shown in Fig. 5.

Table 2 Tensile mechanical properties and mechanical anisotropy of as-forged and heat-treated samples at room temperature

Condition	Direction	YS/MPa	UTS/MPa	EL/%	ΔYS/MPa
As-forged	TD	180±4.7	317±0.6	17.8±0.1	35
	RD	215±6.7	346±0.8	16.0±0.5	
T4	TD	153±4.5	289±1.4	11.8±0.5	29
	RD	182±2.4	307±2.6	8.3±0.5	
T5	TD	240±5.0	355±2.5	8.0±0.1	32
	RD	272±1.6	382±4.7	6.8±0.8	
T6	TD	224±1.6	338±2.7	4.9±0.8	32
	RD	256±12.4	359±8.0	4.2±0.2	

In terms of basal slip, the Schmid factor distributions along the TD and RD are similar with low average Schmid factors (0.17 and 0.16, respectively). When the sample is stretched along the RD, the average Schmid factor for prismatic slip is 0.42 and the fraction of grains with Schmid factor higher than 0.4 accounts for 85%, which indicates that most grains are in soft orientations for prismatic slip. When the sample is stretched along

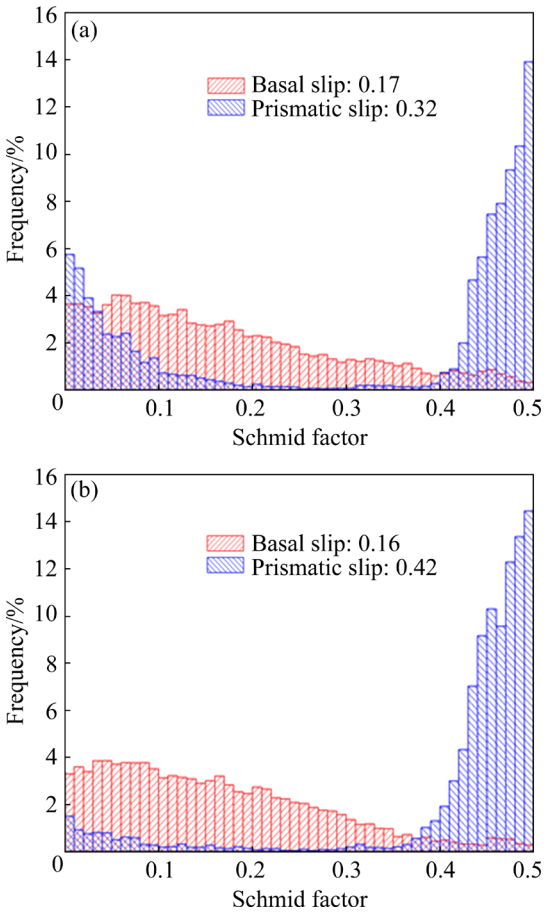

Fig. 5 Schmid factor distribution maps based on basal and prismatic slip for as-forged sample along TD (a) and RD (b)

the TD, there are more grains with Schmid factor between 0 and 0.2 due to the presence of sub-strong basal texture component that is unfavorable for prismatic slip, resulting in a lower average Schmid factor (0.32). According to the previous studies, the CRSS ratio of prismatic and basal slip in the Mg−Al alloys is in the range of 2.0−5.0 [26,29,30]. Therefore, with the corresponding average Schmidt factor ratio less than 2, basal slip dominates the deformation along the TD. And the YS along the RD is higher than that along the TD, because more prismatic slips with higher CRSS are activated along the RD. Besides, T4 sample remains the same texture feature as mentioned above, and aging treatment has a negligible effect on the texture. As a result, the mechanical anisotropy hardly changes after heat treatment.

By comparison, it can be seen from Table 2 that the effect of heat treatment on tensile properties is consistent in two directions, so TD is selected for analysis. Notably, the tensile mechanical properties of the T4 sample are all lower than those of the as-forged sample. Due to the high temperature of isothermal die forging, there are few dynamic precipitates in the as-forged sample, which results in a very limited solid solution strengthening after T4 treatment. Therefore, the decrease in strength caused by grain growth, the reduction in dislocation density and dissolution of β-phase particles during T4 treatment cannot be offset. At the same time, grain coarsening also reduces the EL, from 17.8% to 11.8%. After aging treatment (T5 and T6 treatment), the YS and UTS are obviously improved, but at the cost of a decrease in EL, which is attributed to the precipitation of a large amount of β phases during aging, as shown in Fig. 3.

It is worthwhile to note that the T5 sample possess higher strength and EL than the T6 sample, which is related to aging precipitates. Many studies have shown that DPs play a more critical role in aging hardening because CPs with the plate plane parallel to the basal plane of the matrix are less effective in hindering dislocation slip on the basal plane [3]. Furthermore, it has also been observed that the hardness of the DPs region is higher than that of the CPs region, and a reduction in the area fraction of the DPs region will lead to a decrease in hardness and strength [31−33], which is well consist with the present results. In addition, the relatively coarse DPs are known to be highly susceptible to fracture due to their brittleness [34]. This is demonstrated by the post-fracture microstructure of aged samples in Fig. 6: cracks were mainly formed in the DPs region. Therefore, the loss of EL caused by aging in the as-forged sample (from 17.8% to 8.0%) is higher than that in the T4 sample (from 11.8% to 4.9%) because of the precipitation of more DPs in the former that act as nucleation sites for microcracks during tensile testing, which is similar to the results previously observed in aged AZ80 alloys [33,35].

3.3 Tensile mechanical properties of as-forged and heat-treated samples at elevated temperatures

Figures 7(a) and (b) represent engineering stress−strain curves of the as-forged and heat-treated samples with tensile direction parallel to the TD at 120 and 150 °C, respectively. The corresponding tensile properties are given in Table 3. The strength decreases and the plasticity increases in different degrees with increasing tensile

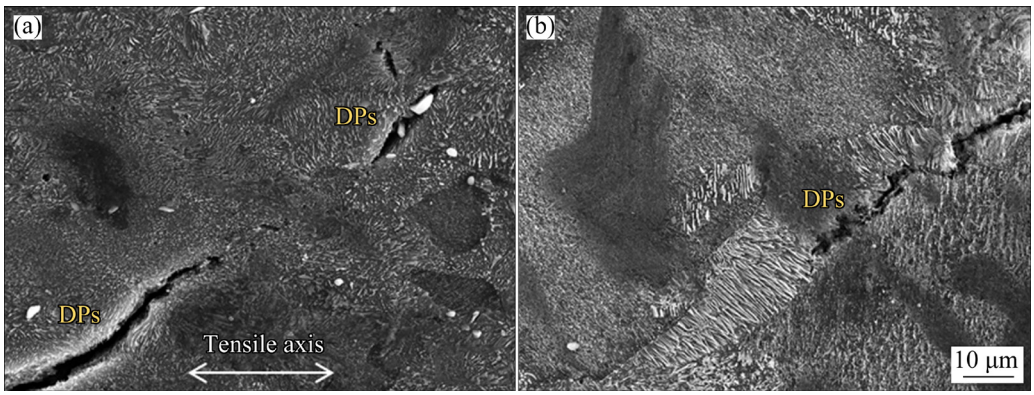

Fig. 6 SEM images of longitudinal cross-sections of tensile fractured T5 (a) and T6 (b) samples at room temperature

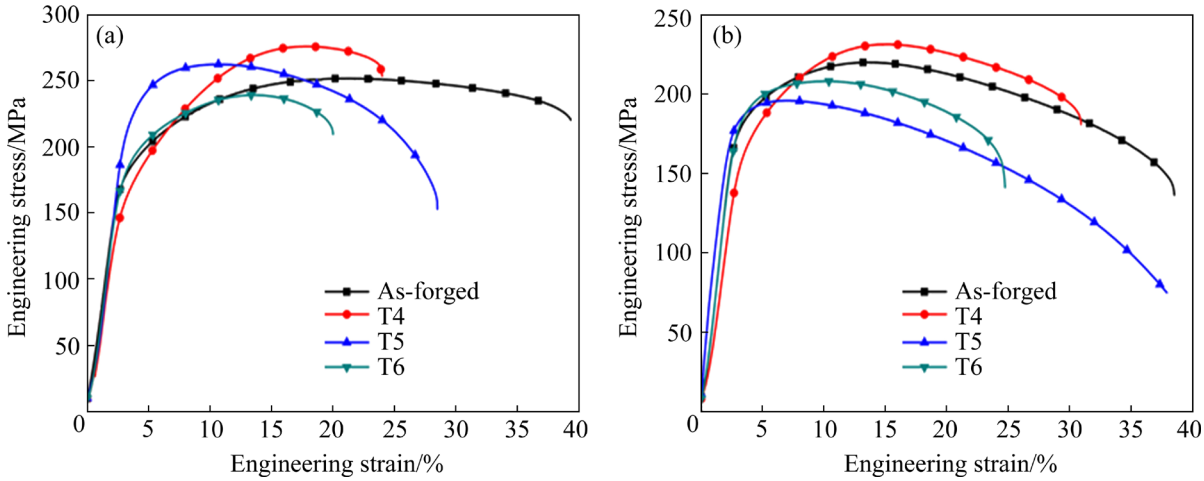

Fig. 7 Tensile engineering stress−strain curves of as-forged and heat-treated samples with loading direction parallel to TD at 120 °C (a) and 150 °C (b)

Table 3 Tensile mechanical properties of as-forged and heat-treated samples with loading direction parallel to TD at 120 and 150 °C

Temperature/°C	Condition	YS/MPa	UTS/MPa	EL/%
120	As-forged	169±0.9	254±4.0	38.0±1.8
	T4	144±4.2	275±0.8	27.5±2.6
	T5	205±0.9	258±4.9	34.1±5.0
	T6	201±4.5	250±3.2	23.8±2.3
150	As-forged	161±3.8	214±6.0	39.7±0.5
	T4	139±0.8	227±4.5	31.3±2.9
	T5	152±3.1	198±1.6	39.5±1.5
	T6	166±5.5	202±6.4	27.6±1.6

temperature. In order to intuitively compare the resultant mechanical properties, variations in YS, UTS and EL as a function of tensile temperature are shown in Fig. 8. In Fig. 8(a), the YS values of the aged samples decrease significantly with increasing temperature. Among them, the YS of the T5 sample decreases more rapidly than that of the T6 sample at elevated temperature, which results in the T5 sample with higher strength at room temperature having similar YS to the T6 sample at 120 °C and lower YS at 150 °C. However, the as-forged and T4 samples only decrease slightly, which is less than 20 MPa even at 150 °C. As a result, the YS of the as-forged sample is close to that of the T6 sample and even higher than that of the T5 sample at 150 °C. It is evident from Fig. 8(b) that all samples show a significant decrease in UTS at elevated temperature except for T4 sample at 120 °C. As for EL, as seen in Fig. 8(c), each sample has a great improvement at 120 °C, but with a slight increase from 120 to 150 °C. It is worth noting that, the EL of the T5 sample increases the most with temperature, and even approaches that of the as-forged sample at 150 °C, while the EL of the T6 sample remains the lowest.

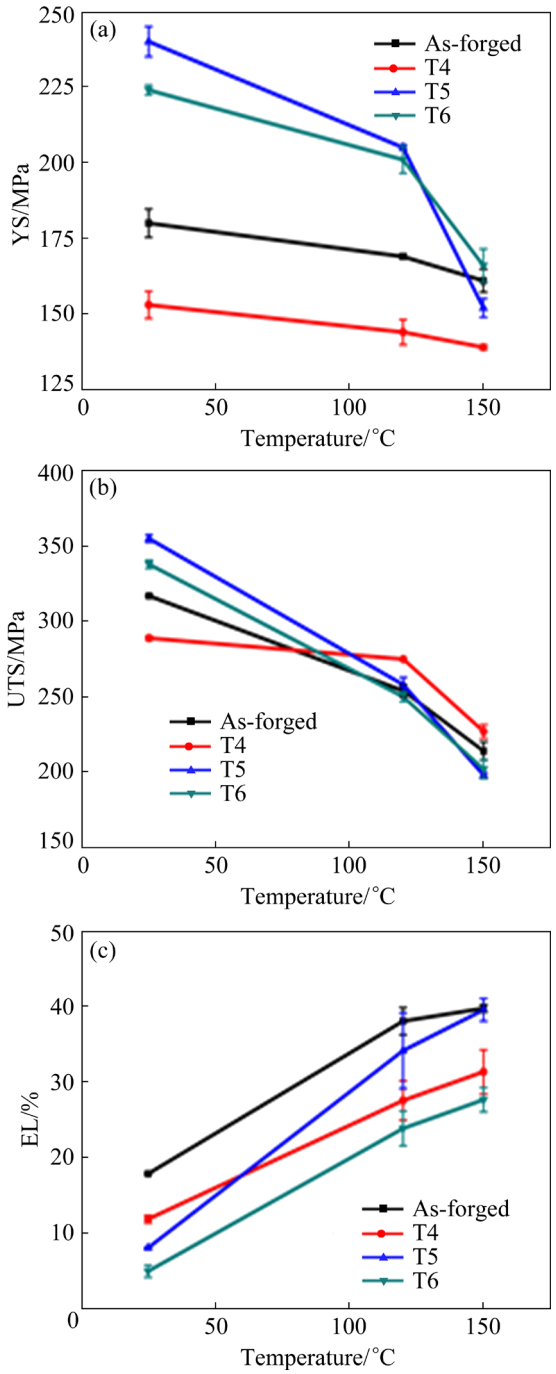

Fig. 8 Variations of YS (a), UTS (b) and EL (c) with tensile temperature in as-forged and heat-treated samples stretched along TD

It is well known that the β-phase has a low melting point (437 °C) and tends to soften and/or coarsen when the temperature is above 120 °C, resulting in a reduction in its ability to block dislocation movement and a corresponding weakening of precipitation strengthening [36], which is the main strengthening mechanism of aged samples at room temperature. Therefore, the strength of aged samples decreases obviously at elevated temperatures. As mentioned above, the dominant deformation mechanism of the TD tensile specimens is basal slip, which is not sensitive to temperature [37]. Moreover, there are few β-phases in the as-forged and T4 samples, so the YS hardly changes with the variation of temperature.

In order to explain the evolution of tensile properties of the T5 sample at elevated temperatures, the SEM images of its longitudinal cross-sections near the tensile fracture surfaces at 150 °C are shown in Fig. 9. It can be seen that grains are significantly elongated along the tensile direction, and microcrack is observed at grain boundary, but not in the DPs region (Fig. 9(a)), suggesting that the softened DPs are not susceptible to becoming microcrack nucleation sites at room temperature. At high magnification (Fig. 9(b)), the DPs region is mainly composed of fine elliptical DPs and relatively coarse irregular phases, while typical cellular structure is not observed and only few fractured lamellar DPs (see the yellow ellipse) along the tensile direction exist. It can be inferred that the softened lamellar DPs were broken during tensile at elevated temperatures, which subsequently became segregated in grain interiors and at grain boundaries and formed coarse irregular

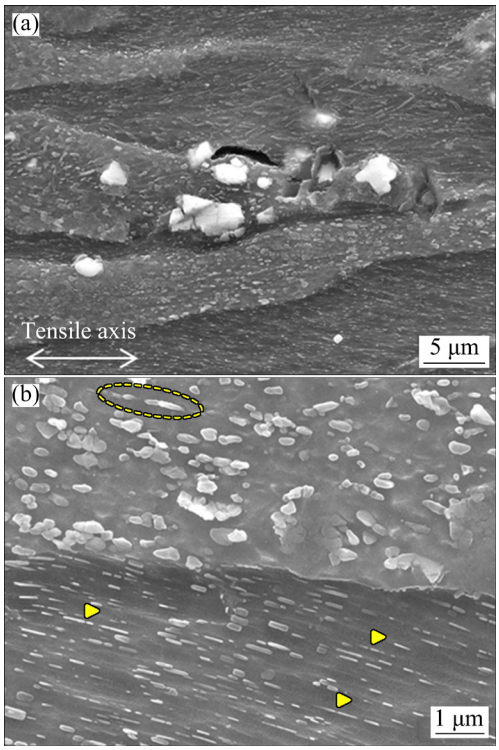

Fig. 9 SEM images of longitudinal cross-sections near tensile fracture surfaces of T5 sample at 150 °C

phases. It has been reported that the softened β-phase particles segregating along grain boundaries can promote grain boundary sliding (GBS) behavior and hence superplasticity in the rolled AZ91 alloy by relaxing intergranular stress incompatibilities [38]. Therefore, the softened DPs and GBS behaviors contribute to the rapid increase of EL in the T5 sample at elevated temperatures. Meanwhile, CPs remain lath-shaped and dispersive, though some of them are broken into multiple pieces (see the yellow triangles in Fig. 9(b)). The evolution of precipitates indicates that CPs have better resistance to high temperature softening during tensile deformation, so the T5 sample exhibits a greater strength decline due to the lower area fraction of CPs.

4 Conclusions

(1) After T4 treatment, the sample of the isothermal die forged AZ80−Ag disk maintained inhomogeneous microstructure and bimodal texture. The microstructure of T5 and T6 samples was dominated by DPs and CPs, and the area fraction of DPs in T5 sample was higher.

(2) The tensile deformation of the as-forged sample was dominated by basal slip along the TD, while prismatic slip contributed more to deformation along the RD, resulting in mechanical anisotropy, which hardly changed after heat treatments.

(3) T5 sample exhibited a superior tensile strength at room temperature to T6 sample, whereas an opposite result was observed at 150 °C. This is mainly because DPs play a more critical role in precipitation hardening at room temperature, but are less resistant to high temperature softening, which also led to a rapid increase in the EL of T5 sample at elevated temperatures.

Acknowledgments

The authors are grateful for the financial support from the National Natural Science Foundation of China (No. 51874367).

References

[1] YANG Zhong, LI Jian-ping, ZHANG Jian-xin, LORIMER G W, ROBSON J. Review on research and development of magnesium alloys [J]. Acta Metallurgica Sinica (English Letters), 2008, 21: 313−328.

[2] ZHAO De-gang, WANG Zhen-qing, ZUO Min, GENG Hao-ran. Effects of heat treatment on microstructure and mechanical properties of extruded AZ80 magnesium alloy [J]. Materials & Design, 2014, 56: 589−593.

[3] NIE Jian-feng. Precipitation and hardening in magnesium alloys [J]. Metallurgical and Materials Transactions A, 2012, 43: 3891−3939.

[4] PEKGULERYUZ M, CELIKIN M. Creep resistance in magnesium alloys [J]. International Materials Reviews, 2010, 55: 197−217.

[5] YU Shi-lun, GAO Yong-hao, LIU Chu-ming, HAN Xiu-zhu. Effect of aging temperature on precipitation behavior and mechanical properties of extruded AZ80−Ag alloy [J]. Journal of Alloys and Compounds, 2015, 646: 431−436.

[6] ZENG Gang, LIU Chu-ming, WAN Ying-chun, GAO Yong-hao, JIANG Shu-nong, CHEN Zhi-yong. Effects of aging temperature on microstructure, tensile and creep properties of ring rolled AZ80−Ag alloy [J]. Materials Science and Engineering: A, 2018, 734: 59−66.

[7] MAO Long-hui, LIU Chu-ming, GAO Yong-hao, HAN Xiu-zhu, JIANG Shu-nong, CHEN Zhi-yong. Microstructure and mechanical anisotropy of the hot rolled Mg−8.1Al−0.7Zn−0.15Ag alloy [J]. Materials Science and Engineering: A, 2017, 701: 7−15.

[8] GRONOSTAJSKI Z, PATER Z, MADEJ L, GONTARZ A, LISIECKI L, LUKASZEK-SOLEK A, LUKSZA J, MRÓZ S, MUSKALSKI Z, MUZYKIEWICZ W, PIETRZYK M, SLIWA R E, TOMCZAK J, WIEWIÓROWSKA S, WINIARSKI G, ZASADZINSKI J, ZIÓLKIEWICZ S. Recent development trends in metal forming [J]. Archives of Civil and Mechanical Engineering, 2019, 19: 898−941.

[9] WANG Qiang, ZHANG Zhi-ming, ZHANG Xing, LI Guo-jun. New extrusion process of Mg alloy automobile wheels [J]. Transactions of Nonferrous Metals Society of China, 2010, 20(S): s599−s603.

[10] HE Hai-lin, HUANG Shi-quan, YI You-ping, GUO Wan-fu. Simulation and experimental research on isothermal forging with semi-closed die and multi-stage-change speed of large AZ80 magnesium alloy support beam [J]. Journal of Materials Processing Technology, 2017, 246: 198−204.

[11] YUAN Lin, ZHAO Zhe, SHI Wen-chao, XU Fu-chang, SHAN De-bin. Isothermal forming of the large-size AZ80A magnesium alloy forging with high mechanical properties [J]. The International Journal of Advanced Manufacturing Technology, 2015, 78: 2037−2047.

[12] WU Yang, CHEN Qiang, XIA Xiang-sheng. Isothermal precision forging of magnesium alloy components with high performance [J]. Procedia Engineering, 2017, 207: 896−901.

[13] SHAN De-bin, XU Wen-chen, HAN Xiu-zhu, HUANG Xiao-lei. Study on isothermal precision forging process of rare earth intensifying magnesium alloy [J]. Materials Science and Engineering: B, 2012, 177: 1698−1702.

[14] UEMATSU Y, TOKAJI K, MATSUMOTO M. Effect of aging treatment on fatigue behaviour in extruded AZ61 and AZ80 magnesium alloys [J]. Materials Science and

Engineering: A, 2009, 517: 138−145.

[15] ZHAO Xi, GAO Peng-cheng, CHEN Gang, WEI Jian-feng, ZHU Zhuang, YAN Fa-fa, ZHANG Zhi-min, WANG Qiang. Effects of aging treatments on low-cycle fatigue behavior of extruded AZ80 for automobile wheel disks [J]. Materials Science and Engineering: A, 2021, 799: 140366.

[16] LIANG Min-jie, ZHENG Jie, LIU Huan, YAO Bao-xing. Microstructure and mechanical properties of AZ31 alloy prepared by cyclic expansion extrusion with asymmetrical extrusion cavity [J]. Transactions of Nonferrous Metals Society of China, 2022, 32: 122−133.

[17] XU Nan, ZHANG Wei-da, CAI Si-qi, ZHUO Yue, SONG Qi-ning, BAO Ye-feng. Microstructure and tensile properties of rapid-cooling friction-stir-welded AZ31B Mg alloy along thickness direction [J]. Transactions of Nonferrous Metals Society of China, 2020, 30: 3254−3262.

[18] KIM S H, LEE J U, KIM Y J, MOON B G, YOU B S, KIM H S, PARK S H. Improvement in extrudability and mechanical properties of AZ91 alloy through extrusion with artificial cooling [J]. Materials Science and Engineering: A, 2017, 703: 1−8.

[19] SUN Jia-peng, YANG Zhen-quan, HAN Jing, LIU Huan, SONG Dan, JIANG Jing-hua, MA Ai-bin. High strength and ductility AZ91 magnesium alloy with multi-heterogenous microstructures prepared by high-temperature ECAP and short-time aging [J]. Materials Science and Engineering: A, 2018, 734: 485−490.

[20] LAI W J, LI Y Y, HSU Y F, TRONG S, WANG W H. Aging behaviour and precipitate morphologies in Mg−7.7Al−0.5Zn−0.3Mn (wt.%) alloy [J]. Journal of Alloys and Compounds, 2009, 476: 118−124.

[21] CELOTTO S, BASTOW T J. Study of precipitation in aged binary Mg−Al and ternary Mg−Al−Zn alloys using ^{27}Al NMR spectroscopy [J]. Acta Materialia, 2001, 49: 41−51.

[22] KIM S H, LEE J U, KIM Y J, BAE J H, YOU B S, PARK S H. Accelerated precipitation behavior of cast Mg−Al−Zn alloy by grain refinement [J]. Journal of Materials Science & Technology, 2018, 34: 265−276.

[23] ROBSON J D. Modeling competitive continuous and discontinuous precipitation [J]. Acta Materialia, 2013, 61: 7781−7790.

[24] ZHANG Ming-xing, KELLY P M. Crystallography of $Mg_{17}Al_{12}$ precipitates in AZ91D alloy [J]. Scripta Materialia, 2003, 48: 647−652.

[25] AGNEW S R, TOMÉ C N, BROWN D W, HOLDEN T M, VOGEL S C. Study of slip mechanisms in a magnesium alloy by neutron diffraction and modeling [J]. Scripta Materialia, 2003, 48: 1003−1008.

[26] HUA X, LV F, QIAO H, ZHANG P, DUAN Q Q, WANG Q, WU P D, LI S X, ZHANG Z F. The anisotropy and diverse mechanical properties of rolled Mg−3%Al− 1%Zn alloy [J]. Materials Science and Engineering: A, 2014, 618: 523−532.

[27] SONG Bo, DU Zhi-wen, YANG Qing-shan, GUO Ning, GUO Sheng-feng, YU Jin-cheng, XIN Ren-long. Effect of pre-rolling path on mechanical properties of rolled ZK60 alloys [J]. Transactions of Nonferrous Metals Society of China, 2021, 31: 1322−1338.

[28] HE Jun-jie, MAO Yong, GAO Yu-ping, XIONG Kai, JIANG Bin, PAN Fu-sheng. Effect of rolling paths and pass reductions on the microstructure and texture evolutions of AZ31 sheet with an initial asymmetrical texture distribution [J]. Journal of Alloys and Compounds, 2019, 786: 394−408.

[29] STANFORD N, GENG Jie, CHUN Y B, DAVIES C H J, NIE Jian-feng, BARNETT M R. Effect of plate-shaped particle distributions on the deformation behaviour of magnesium alloy AZ91 in tension and compression [J]. Acta Materialia, 2012, 60: 218−228.

[30] WEI Jian-sheng, LIU Chu-ming, WAN Ying-chun, SHAO Jian-bo, HAN Xiu-zhu, ZHANG Gao-long. Strengthening against $\{10\bar{1}2\}$ twinning by discontinuous and continuous precipitate in a strongly textured Mg−9Al alloy [J]. Materials Characterization, 2020, 167: 110523.

[31] ZHANG Ke-long, LI Hui-zhong, LIANG Xiao-peng, CHEN Zhi, WANG Li. Discontinuous and continuous precipitation characteristics and mechanical properties of a AZ80A magnesium alloy at different aging temperatures [J]. Materials Characterization, 2020, 161: 110146.

[32] LEE J U, KIM S H, KIM Y J, PARK S H. Effects of homogenization time on aging behavior and mechanical properties of AZ91 alloy [J]. Materials Science and Engineering: A, 2018, 714: 49−58.

[33] LEE G M, LEE J U, PARK S H. Effects of post-heat treatment on microstructure, tensile properties, and bending properties of extruded AZ80 alloy [J]. Journal of Materials Research and Technology, 2021, 12: 1039−1050.

[34] LEE S, LEE S H, KIM D H. Effect of Y, Sr, and Nd additions on the microstructure and microfracture mechanism of squeeze-cast AZ91−X magnesium alloys [J]. Metallurgical and Materials Transactions A, 1998, 29: 1221−1235.

[35] ZHOU Xiao-jie, ZHANG Jian, CHEN Xiao-min, ZHANG Xu, LI Meng-jia. Fabrication of high-strength AZ80 alloys via multidirectional forging in air with no need of ageing treatment [J]. Journal of Alloys and Compounds, 2019, 787: 551−559.

[36] MO Ning, TAN Qi-yang, BERMINGHAM M, HUANG Yuan-ding, DIERINGA H, HORT N, ZHANG Ming-xing. Current development of creep-resistant magnesium cast alloys: A review [J]. Materials & Design, 2018, 155: 422−442.

[37] CHAPUIS A, DRIVER J H. Temperature dependency of slip and twinning in plane strain compressed magnesium single crystals [J]. Acta Materialia, 2011, 59: 1986−1994.

[38] ZHA Min, ZHANG Hong-min, WANG Cheng, WANG Hui-yuan, ZAHNG En-bo, JIANG Qi-chuan. Prominent role of a high volume fraction of $Mg_{17}Al_{12}$ particles on tensile behaviors of rolled Mg−Al−Zn alloys [J]. Journal of Alloys and Compounds, 2017, 728: 682−693.

热处理对大规格等温模锻 AZ80−Ag 镁合金机匣显微组织和拉伸力学性能的影响

陈飞腾[1]，蒋树农[1]，陈志永[1]，刘楚明[1,2]

1. 中南大学 材料科学与工程学院，长沙 410083；
2. 湖南科技大学 材料科学与工程学院，湘潭 411201

摘　要：研究大规格等温模锻 AZ80−Ag 镁合金机匣在不同热处理条件下的组织演变和拉伸力学性能。采用扫描电镜和电子背散射衍射对合金的显微组织进行表征，并测试其在室温、120 和 150 ℃下的拉伸力学性能。结果表明，室温下强化作用更强的不连续析出相在 T5 样品中的面积分数高于 T6 样品的面积分数。因此，T5 样品的析出强化作用更强，室温抗拉强度最高。但随着温度的升高，T5 样品的抗拉强度迅速下降，在 150 ℃时低于 T6 样品甚至锻造态样品的抗拉强度。这是由于不连续析出相的抗高温软化能力低于连续析出相的抗高温软化能力。

关键词：AZ80−Ag 合金；热处理；高温拉伸性能；不连续析出相；析出强化

(Edited by Wei-ping CHEN)